X-ray generation in a cavity heated by 1.3- or 0.44-μm laser light. I. Time-integrated measurements

S. Sakabe,* R. Sigel, G. D. Tsakiris, I. B. Földes,† and P. Herrmann
Max-Planck-Institut für Quantenoptik, D-8046 Garching, Federal Republic of Germany
(Received 17 May 1988)

The x-ray radiation generated in gold cavities (diameter 250–1000 μm) that were heated by 300-ps laser light pulses with a wavelength of 1.3 or 0.44 μm has been experimentally investigated. The absorbed laser intensity, averaged over the inner surface of the cavity, was varied in the range 2×10^{12}–5×10^{13} W cm^{-2}. Laser light absorption was measured with an Ulbricht box. The cavity heating process was investigated by x-ray pinhole photography and time-resolved optical shadowgraphy. The radiant energy flux in the cavity and its spectral distribution were measured at three different locations in the cavity by spatially resolving transmission grating spectrometers. The experiments performed at the wavelength of 1.3 μm show low ($\sim$30%) laser light absorption, delocalized heating due to refraction of laser light, and hard x-ray emission due to fast electron generation in the cavity. The 0.44-μm experiments show $>80\%$ absorption, localized heating at the laser-irradiated back wall of the cavity, and comparatively low hard x-ray emission. A maximum brightness temperature of 1.5×10^6 K was measured in the smallest cavities.

I. INTRODUCTION

Modern pulsed power sources, in particular, lasers, make it possible to study high-temperature hydrodynamic phenomena[1] in the laboratory. Of particular interest is the generation of intense blackbody radiation in small cavities of high-Z material[2,3] either for basic investigations of the state of matter at high temperatures and densities or for inertial confinement fusion.[4,5] Recently, several experimental investigations related to the laser heating of cavities have appeared in the literature.[6–11]

The ideal case of cavity heating analyzed in our previous theoretical work[2,3] assumes complete thermalization of the laser radiation into x rays, uniform deposition of laser energy on the inner wall of the cavity, and the establishment of complete thermodynamic equilibrium in the cavity. The actual situation in experiments is much more complex. As is well known from experimental and theoretical investigations with planar targets, the conversion of laser light into x rays is, in general, incomplete and depends on the laser wavelength and intensity.[12–22] The lower the x-ray conversion efficiency the more energy will appear in the cavity in other forms, in particular, as kinetic and internal energy of a hot plasma whose properties may be dominated by fast electrons generated during high-intensity laser-plasma interaction. The rapid expansion of this plasma into the cavity may give rise to serious complications such as premature plasma filling of the cavity with subsequent rejection of the laser light. Such complications are expected especially if long-wavelength laser light is used for cavity irradiation and if—as is the case for single-beam experiments as the present one—the laser energy is deposited on a small fraction of the inner cavity surface area at a correspondingly high laser intensity. Furthermore, as our previous work[2,3] has shown, the establishment of equilibrium conditions in the cavity is a matter of the availability of energetic laser pulses.

The present investigation, though more comprehensive than the published works,[6–11] is still mainly an experimental investigation aiming at the identification of problems associated with the laser heating of cavities. The role of the laser wavelength is studied by using laser pulses at the two wavelengths of 1.3 and 0.44 μm. Accurate absorption measurements are made at both wavelengths. The dependence of the x-ray flux in the cavity on the average absorbed laser intensity is investigated by varying the cavity size. The heating processes in the cavity interior are studied by x-ray pinhole photography and the uniformity of energy deposition by time-resolved optical shadowgraphy using thin-walled cavities. The radiant energy flux and its spectral distribution are measured at three different locations in the cavity in an attempt to identify the primary source of x rays and the relative importance of wall and volume emission. As we shall see the observations indicate strong differences in the physical process of cavity heating at the two laser wavelengths. However, for cavities irradiated with laser light of the shorter wavelength, the situation seems to approach the ideal case of an empty, radiation filled cavity which is amenable to analytical modeling.

The results of our study of cavity heating with laser light are presented in three parts (papers I–III). This is paper I and presents the results of the time-integrated measurements (they have been documented in somewhat more detail elsewhere[23]). In paper II (Ref. 24) we present the time-resolved spectral measurements obtained with an x-ray streak camera and in paper III (Ref. 25) we compare the results with theoretical predictions which are based on self-similar solutions of the hydrodynamic equations with radiative heat conduction.[2,3]

II. EXPERIMENTAL SETUP

The cavities used in the present experiment are made of gold and have a diameter (D) of 250 to 1000 μm. A typical cavity has two holes. One is for the laser light injection (we call it the laser hole) and the other is for the radiation measurement (the diagnostic hole). The diameters of the laser hole (D_L) and diagnostic hole (D_d) are in the range 145–530 μm and 98–234 μm with the ratios $D_L/D \cong 0.6$ and $D_d/D \cong 0.4$, respectively. The wall thickness of the cavities was usually 2 μm. This allowed us to study the expansion dynamics of the cavity by optical shadowgraphy and the generation of hard x-rays in the cavity by pinhole photography, allowing conclusions on the uniformity of cavity heating. The cavities were carefully handled and chemically cleaned in order to avoid impurities on the inner surface of the cavity.

Figure 1(a) shows the experimental arrangement. The cavities were irradiated by 300-ps laser pulses [full width at half maximum (FWHM)], emitted by the Asterix III iodine laser system either at the fundamental wavelength of 1.3 μm or at the third harmonic wavelength of 0.44 μm. The laser beam was focused by an aspheric lens with an effective f number of 2.5. The pointing accuracy of the laser beam was approximately ± 30 μm. The average laser flux in the cavity was changed by varying the cavity size at fixed laser energy (~ 20 J for a 0.44-μm laser and ~ 80 J for 1.3 μm). Its value, calculated from the absorbed laser energy, pulse duration, and the inner surface of the cavity was in the range 2×10^{12} to 5×10^{13} W/cm^2. At the directly laser irradiated area at the back wall of the cavity the laser flux was 5×10^{13} to 5×10^{15} W/cm^2.

The laser radiation rejected by the cavity target was monitored by an Ulbricht (integrating) box photometer[26] fitted into the target chamber. Optical shadowgraphy[27] provided a photograph of the expanding cavity at 7 ns after the main laser pulse with an exposure time of 3 ps. The x-ray pinhole cameras (PHC) were equipped with Pt pinholes of 30 μm diam, with Cu and Al filters 1–2-μ and 5–10-μm thick, respectively, and with film as detector. In order to register the emission of relatively soft x rays (0.7 to 3 keV) and hard x rays (3 to 10 keV) at the same time, Kodak 101 film (at the front) and Kodak SB2 film were stacked behind each other. The Kodak 101 film in front of the Kodak SB2 film acts not only as detector, but also as an attenuator for soft x rays. The substrate of the Kodak 101 film consists mainly of cellulose acetate film with a thickness of 125 μm. We have estimated, taking the spectral sensitivity of SB2 film and the characteristics of this additional filter into account, that the SB2 film registers x-ray images in the spectral range 3–10 keV.

Absolute spectrally resolved measurements of the soft x rays emitted from the cavity were made with three transmission-grating spectrometers (TGS).[28] The transmission gratings[29] have 1000 free-standing gold bars per millimeter integrated into a pinhole with 25 μm diameter to give spatial resolution. The spectral resolution of the TGS was 3 Å for a 50-μm-diam source. In the TGS the gratings were mounted in such a manner that they provided dispersion in the vertical and spatial resolution in the horizontal direction. Kodak 101 film was used as detector. It has been absolutely calibrated with the help of a bolometer in the wavelength range of 10–100 Å.[28,30]

In Fig. 1(b) the cavity wall elements observed by the TGS's are shown together with the configuration of laser irradiation. The focus of the laser beam was located in the plane of the laser hole. The TGS1 observes the back wall (laser irradiated) and the side wall (not laser irradiated) through the diagnostic and laser hole, respectively. The TGS2 observes almost the same area on the side wall through the diagnostic hole as does the TGSl through the laser hole. The TGS3 observes through the diagnostic hole and the laser hole and would register no radiation

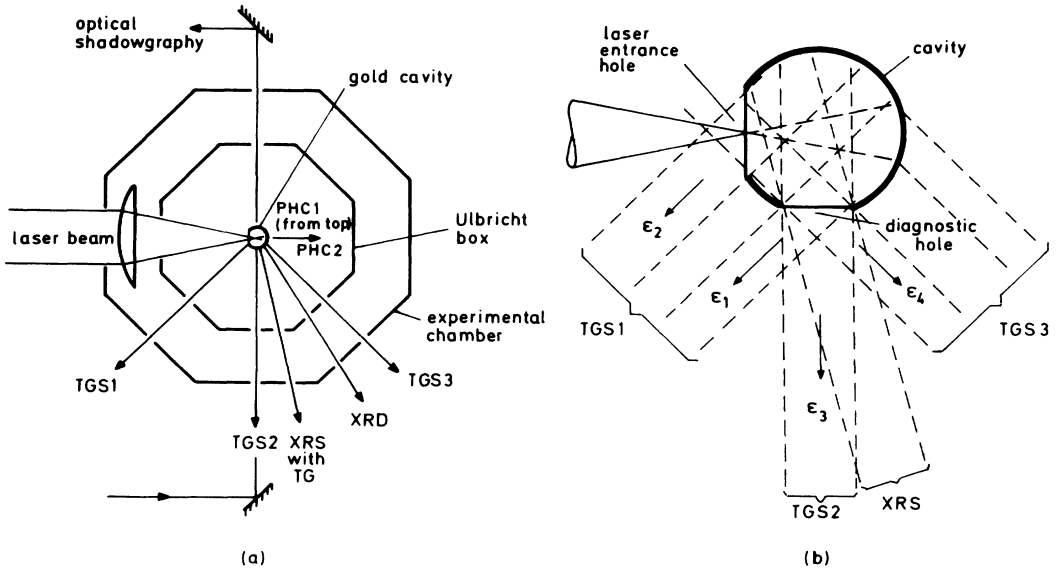

FIG. 1. (a) Experimental setup. (b) Cavity observation.

through the diagnostic hole if the heated cavity remained completely empty. The TGS3 registers also radiation from the outer surface of the laser-irradiated back wall. We note that in addition an x-ray streak camera (XRSC) combined with a transmission grating (TG) was used to measure simultaneously time-resolved spectra. The results obtained with this diagnostic will be discussed in paper II.

III. EXPERIMENTAL RESULTS

A. Laser light absorption

The results of the absorption measurements are shown in Fig. 2. It can be immediately seen that the absorption for the 0.44-μm laser irradiation (crosses) is 80–95 %, rather independent on cavity size. The absorption is even higher than the absorption of planar targets which is typically 70–80 %. The enhanced absorption is attributed to the trapping of laser light in the cavity.

In the case of 1.3-μm irradiation (open circles) the absorption decreases from 80% to 30% as the cavity size is reduced from 1000 to 270 μm (corresponding to an increase of the laser intensity from 2×10^{14} to 3×10^{15} W/cm^2 at the back wall). The absorption of planar targets is 30–40 % in this intensity range. The ~80% absorption in the large cavities greatly exceeds that of planar targets showing the efficient increase of absorption due to the closed geometry of the cavities. The absorption of the small cavities (~30%) is approximately equal to that of a planar target; in fact, in several shots it was even lower than that of the corresponding planar targets. The small cavities and their laser holes were obviously so small, that the laser light could not be effectively injected because of plasma closure of the laser hole and the plasma filling of the cavity. A more detailed discussion of the absorption measurements and their interpretation is given elsewhere.[31]

B. X-ray pinhole photography

X-ray photographs of the cavities obtained with the help of the pinhole cameras are presented in Fig. 3. The photographs in the upper row were registered by the Kodak 101 film and were exposed by the very soft x-ray radiation (approximately 0.7 to 3 keV). The photographs in the lower row were obtained in the same shots on the Kodak SB2 film stacked behind the 101 film; this film was exposed by the harder x rays (approximately 3 to 10 keV). Shown are isodensity contours obtained after digitization and computer processing of the films. Overlaid are the contours of the cavities as seen from the direction of the pinholes. The photographs shown in Figs. 3(a) and 3(b) were taken by PHC1 located above the cavity and the photographs shown in Fig. 3(c) by PHC2 located behind the cavity at 45° from the horizontal plane (compare Fig. 1).

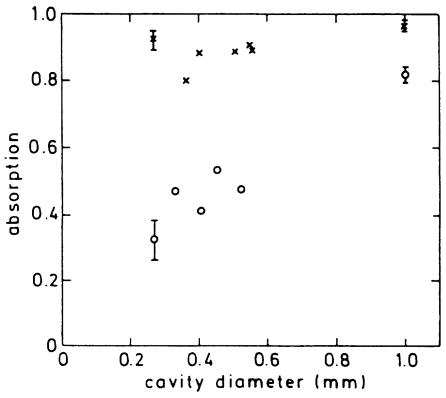

FIG. 2. Laser absorption in cavities (○, 1.3-μm; ×, 0.44-μm laser light).

Prominent features seen in the top row of Fig. 3 are the emission areas near the laser hole (LH) and the diagnostic hole (DH). This emission is caused by the plasma streaming out of the holes during the cooling of the cavities. The emitted x rays are very soft and are not registered by the SB2 film (lower row).

Another emission area is located near the back wall (BW) inside the cavity. It is quite pronounced in the case of the 0.44-μm irradiated cavity shown in Fig. 3(a) and is seen on both films. Because it appears in the area where the back wall is expected to intercept the laser beam it is attributed to the hot plasma formed by direct heating of the back wall by the laser beam. The harder part ($h\nu \geq 2$ keV) of the x-ray emission from this plasma penetrates the wall of the cavity and causes an exposure on both films.

In experiments with small cavities irradiated by 0.44-μm laser light, such as Fig. 3(a), emission is also seen at the rear side of the back wall (RW) from a region located outside the original cavity volume. This emission is attributed to a combination of burnthrough and geometrical thinning of the wall as it is pushed into the direction of the laser beam. This is not unexpected because the heating of the back wall by the laser light is much more intense than the average heating in the cavity. It should be noted that the emission is very soft and is not registered by the SB2 film.

Figure 3(a) shows also an unexpected feature, the so-called spot emission (S). It was actually observed in all experiments, but its intensity increased for small cavities and for 1.3-μm irradiation. It is usually quite prominent on the 101 film but less evident or even absent on the SB2 film. One may speculate that this emission is connected with a hitherto unexplained discharge phenomenon initiated by the generation of fast electrons in the cavity; however, this has to be confirmed by further investigation.

Except for the spot emission, the observations mentioned so far are consistent with a normal scenario where cavity heating occurs via a source of primary x rays at the laser heated back wall. This normal behavior is found in the cavities heated by 0.44-μm laser light, even for the rather small cavity shown in Fig. 3(a). The situation becomes, however, considerably more complicated in the case of small cavities irradiated by 1.3μm laser light. This is seen by comparing the two experiments shown in Figs. 3(a), 3(b), and 3(c), respectively.

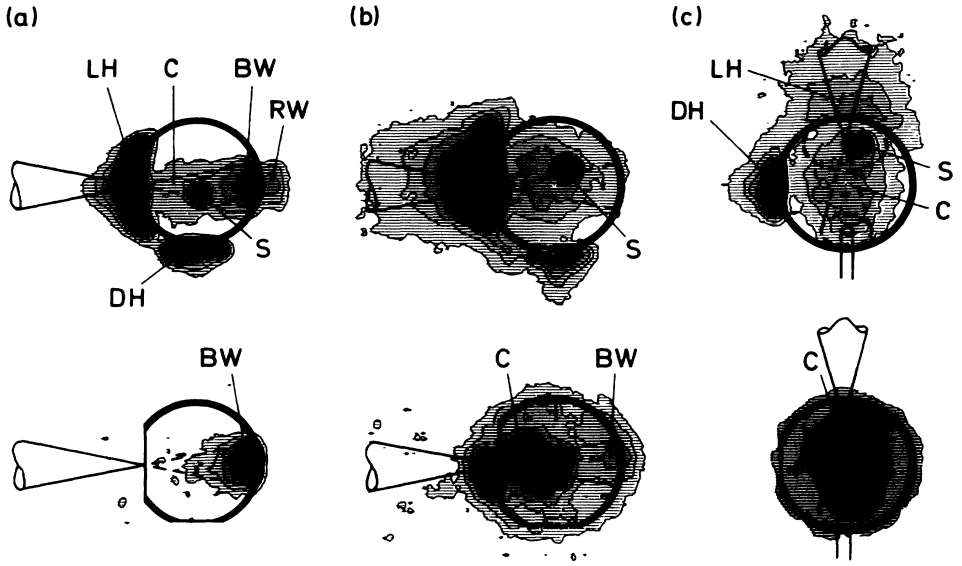

FIG. 3. X-ray pinhole photographs (isodensity contours) of laser-heated cavities. Upper row: Kodak 101-01 films exposed by relatively soft (0.7–3 keV) x rays. Lower row: SB2 films stacked behind the Kodak 101-01 film and exposed simultaneously by harder x rays (3–10 keV). For explanation of the symbols see text. (a) 297-μm-diam cavity heated by 0.44-μm laser light. Pinhole camera PHC1 (from top). Filter 1-μm-thick copper. Laser energy 24 J. (b) 328-μm-diam cavity heated by 1.3-μm laser light. Pinhole camera PHC1 (from top). Filter 1-μm-thick copper. Laser energy 63 J. (c) Same shot as (b); however, cavity observed by pinhole camera PHC2 (from rear side at 45° to the horizontal plane). Filter 1-μm-thick copper.

Perhaps the most instructive difference between the two experiments shown in Fig. 3 concerns the so-called center emission (C), i.e., the emission of x rays from the central region through the wall of the cavity. Whereas in Fig. 3(a) only a spurious center emission may be recognized, it becomes a dominant feature in the 1.3-μm irradiation experiment, especially on the SB2 film (for a 250-μm-diam cavity the SB2 film was overexposed). It extends up to the periphery of the cavity where it is sharply bounded. The center emission (C) can be distinguished from the spot emission (S) with the help of the pair of stereoscopic photographs of the same shot shown in Figs. 3(b) and 3(c). A closer inspection shows that the center emission is a volume emission from the central region of the cavity and the spot emission a wall emission from the top of the cavity.

The center emission is considered to be a consequence of the plasma filling of the cavity. Because the critical density for 1ω laser light is nine times lower than for 3ω laser light, it is expected that filling effects are much more important in 1.3-μm experiments. As the cavity fills with plasma the laser beam will be refracted and reflected by the plasma and prevented from reaching the back wall of the cavity. Indeed, the very pronounced back-wall emission (BW) seen in Fig. 3(a) is not observed in Fig. 3(b). During the filling of the cavity the laser plasma interaction zone which is considered as the source of the hard x rays observed through the wall of the cavity, shifts into the direction of the laser hole and causes the center emission. In small cavities as the one shown in Fig. 3(b) hard x rays are observed even from the laser hole. Possibly the plasma density exceeds the critical density in the laser hole during the laser pulse and causes the strong reflection losses noted above.

The details of the plasma filling of the cavity may be quite complicated. Experience with CO_2 laser-heated cavities suggests the generation of magnetic fields.[32] In addition, parametric instabilities may be excited with the consequence of an enhanced plasma temperature and of fast-electron generation. The emission of hard x rays from all over the cavity might be an indication of such effects. A possible candidate is stimulated Raman scattering, recently reported from laser-heated cavities.[33,34]

C. Optical shadowgraphy

Figure 4 (lower row) shows optical shadowgrams of two laser-heated cavities irradiated with 0.44-μm [Fig. 4(a)] and 1.3-μm [Fig. 4(b)] laser light, respectively. The shadowgrams were exposed 7 ns after cavity irradiation by the main laser pulse. The shadowgrams shown in the upper row were taken before the main laser irradiation; thus the original shape of the cavity can be seen. The cavities have a wall thickness of 2 μm.

If the diameter of the shadow at 7 ns is compared with the original diameter of the cavity, it is seen that it moves outward with a large velocity. For the smallest cavities used in this investigation, velocities up to about 4×10^6 cm s^{-1} were measured. This is due to the acceleration of the wall material by the large pressure generated by the diffusion of radiation into the wall. The wall acceleration and its relation to x-ray confinement in the cavity has been discussed elsewhere.[9,35] Here we are mainly in-

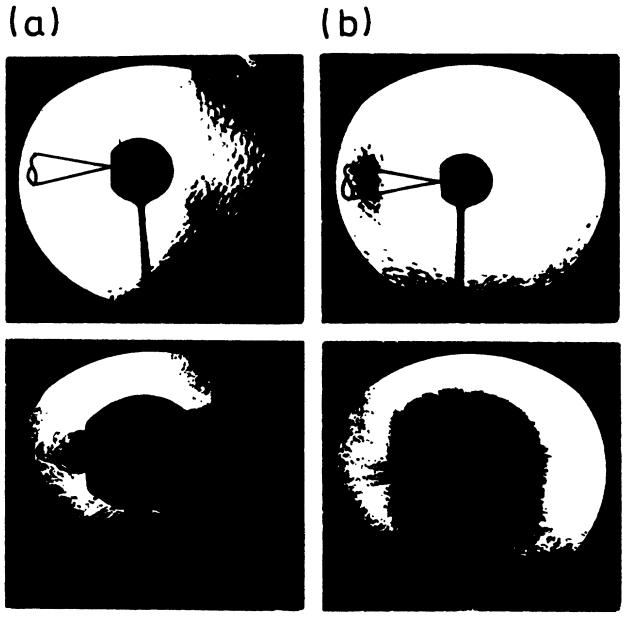

FIG. 4. Optical shadowgrams of two laser-heated cavities exposed by a dye-laser pulse ($\lambda=0.58$ μm) of 3 ps duration. The cavities have a 2-μm-thick gold wall. Upper row: Cavity before irradiation. Lower row: Shadowgram of the expanding cavity 7 ns after the maximum of the heating laser pulse. (a) Cavity with 467 μm diameter heated by 0.44-μm laser light. (b) Cavity with 406 μm diameter heated by 1.3-μm laser light.

terested in the symmetry of the cavity expansion as an indicator of the uniformity of heating in its interior. Let us consider first the 0.44-μm experiment [Fig. 4(a)]. The x-ray pinhole photography has shown that in this case a strong x-ray source is generated through the absorption of the laser beam at the rear wall of the cavity. The x rays emitted by this source will heat the remaining part of the cavity wall, causing an outward acceleration. The expected uniform and spherical expansion is indeed observed for this cavity with 467 μm diameter. As one might expect, the rear wall of the cavity is more strongly accelerated in the laser-irradiated region. The same behavior is also seen in all 0.44-μm experiments with larger cavities. The expansion velocity decreases, of course, with cavity size because the average intensity on the cavity walls decreases.

The cavity heated with 1.3-μm laser light [Fig. 4(b)] does not show such a smooth outer boundary during expansion as in the case of 0.44-μm heating. Rather the boundary is diffuse and carries fine-scale and jetlike structures seen also on massive targets.[36–38] Possibly these phenomena have to do with unipolar arcing.[39,40] A preferential acceleration of the back wall is not observed unless the cavity diameter is larger than about 500 μm. This is consistent with our interpretation of the x-ray photographs.

At both wavelengths the photographs taken with the smallest cavities[23,35] give the impression that the shadow is cast by a plasma atmosphere surrounding the cavity. The structures observed in this atmosphere resemble those observed on open targets at long laser wavelength and high intensity[41,42] generally attributed to fast-electron and magnetic-field generation.

D. Time-integrated spectral measurements

1. *Type of spectra and data reduction*

Spatially resolved, time-integrated spectra obtained simultaneously by the three transmission grating spectrographs TGS 1–3 are presented in Fig. 5. Shown are isodensity contours obtained after digitization and computer processing of the films.

Figure 5(a) shows the case of a medium-size cavity irradiated with 0.44-μm laser light. TGS1 registers the radiation from the sidewall through the laser hole and the very intense radiation from the laser-irradiated area on the back wall of the cavity. TGS2 "sees" the radiation from the side wall through the diagnostic hole and weaker spectra from the laser hole and from the outer side of the back wall of the cavity. TGS3 registers some radiation from the diagnostic hole even though the line of sight passes through the laser hole and is not intercepted by the wall of the cavity. In addition the softer and weaker spectrum of the radiation emitted from the outer side of the back wall of the cavity is seen.

Figure 5(b) shows the case of a similar size cavity irradiated by 1.3-μ laser light. A closer inspection reveals several features which correlate well with the observations discussed above. For example, the strong difference in intensity between the laser-irradiated back wall and the side wall observed by TGS1 is not present in the 1.3-μm irradiation experiment. Also, the spectrum produced by the outer side of the back wall is not as pronounced as before. These observations suggest again that a well-defined laser spot on the back wall does not exist in a cavity irradiated by 1.3-μm laser light. Other observations are that the spectra registered along the line of sight passing freely through the cavity (TGS3) and from the entrance hole (TGS2) tend to become stronger and harder. Also a much stronger background of radiation is observed. The film density was converted into the spectral energy density ϵ_λ of the source, taking into account the geometry of the TGS and cavity, the grating dispersion and efficiency,[29] and the spectral sensitivity of the film.[28,30] It was assumed that the observed wall elements emit according to Lamberts cosine law. At a given wavelength the film density was integrated across the spectrum between limits given by the projection of the source onto the film pulse pinhole diffraction (the latter correction is only of importance for the longest wavelengths). The background on the film was subtracted; this correction is important in the vicinity of the zeroth order where an overlapping of the zeroth order and the spectrum occurs.

2. *Spectra of the laser-irradiated area and of the side wall*

Unfolded spectra are shown in Figs. 6(a) and 6(b) for 0.44-μm (left-hand side) and 1.3-μm (right-hand side) ir-

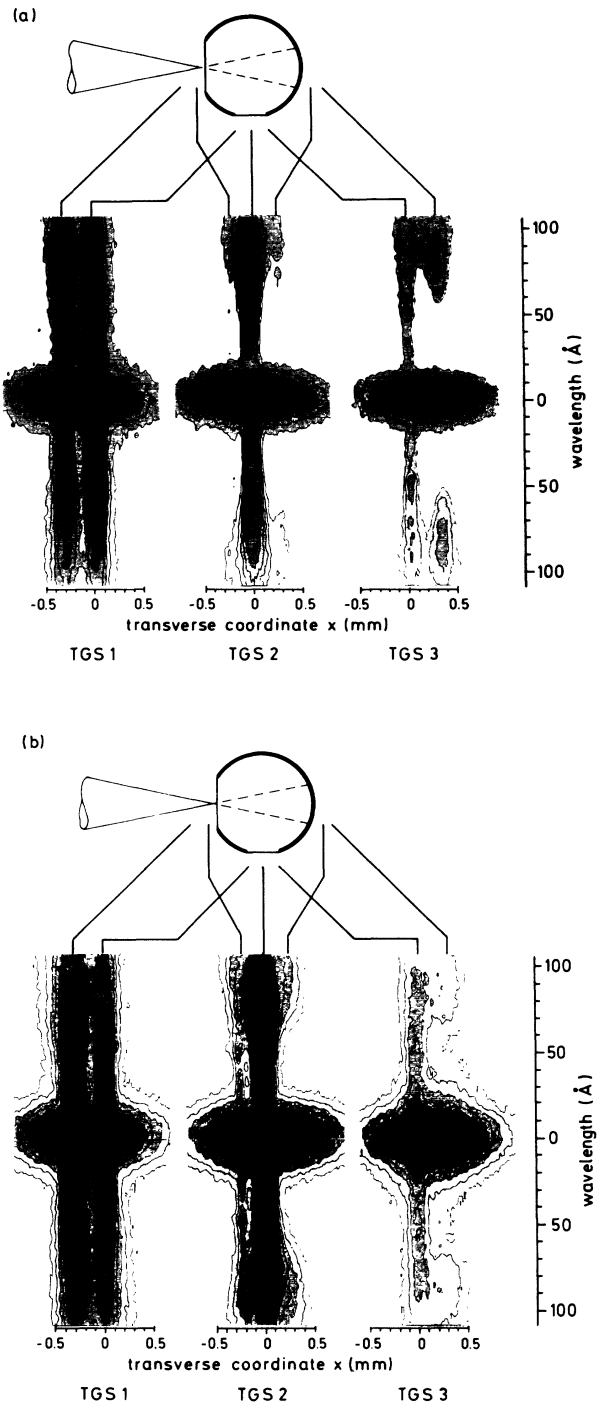

FIG. 5. Soft-x-ray spectra from laser-heated cavities registered by the three transmission grating spectrometers TGS 1–3 on Kodak 101-01 film. Shown are isodensity contours obtained by digitization and computer processing of the films. For clarity the spectra were stretched in the horizontal direction by a factor of 2. As a result the pinhole image of the diagnostic hole formed in zeroth order by the pinhole-grating combination appears elliptical rather than spherical. The transverse coordinate x gives distances in the plane of the cavity. (a) Cavity heated by 0.44-μm laser light (cavity diameter 467 μm, incident energy 22.9 J). (b) Cavity heated by 1.3-μm laser (cavity diameter 519 μm, incident energy 81.5 J).

radiation and two different absorbed laser fluxes. Figure 6(a) relates to the laser-irradiated area on the rear wall of the cavity, Fig. 6(b) to the side wall (see symbols). For comparison, Planck spectra are also shown for the indicated temperatures, calculated assuming an emission time of 300 ps.

The spectra from the laser-irradiated area [Fig. 6(a)] are more intense in the case of 0.44-μm irradiation (by a factor of about 6 for equally absorbed laser flux). This is in agreement with the pinhole photography and optical shadowgraphy observations which have shown that localized heating at the rear wall of the cavity takes place only in the case of 0.44-μm irradiation. Another difference is that the 1.3-μm spectra tend to be harder, particularly for the highest applied laser fluxes.

The spectra of the side wall have been measured through the laser hole [solid line Fig. 6(b)] and the diagnostic hole (dashed line). Though the grating, the observation angle, and the hole size are different there is, in general, a good agreement of the height of the peak at $\sim$20 Å, except for the 1.3-μm irradiation at the highest laser flux. In this case the measured spectral energy density measured through the diagnostic hole is lower by a factor of about 2. The cause of this observation is not known; one of the possible explanations is that material evaporated from the edge of the diagnostic hole (which is small for the small cavities used in the high intensity case) partly absorbs radiation from the interior of the cavity. In the range of long wavelength (50–100 Å) the diagnostic hole tends to radiate generally somewhat more strongly by a factor of 1–2. The excess radiation (compared to a Planckian) observed through both holes in this spectral range is probably generated as the cavity cools after termination of the laser pulse.

The spectra emitted by the side wall (and those by the back wall as well) show two characteristic maxima near 20–30 Å and 40–50 Å. They are attributed to transitions in the N and O band of multiply ionized gold. We have shown previously[8] that the occurrence of structures in the spectrum is expected for the conditions of this experiment. This is due to the lack of complete equilibrium in the cavity, i.e., more precisely to the fact that the optical thickness of the heated wall material is not yet large for all wavelengths. The observed maxima as well as the relative strength and shift with increasing laser flux have been qualitatively reproduced by model calculations. Here we shall not repeat this discussion but concentrate on the spectrally integrated x-ray flux in the cavity for a comparison with theory.

3. *Wall versus volume emission*

Besides wall emission (more precisely the emission from the optically thick radiation heat wave which forms in the wall of the cavity) volume emission from the cavity can also contribute to the measured spectra. A possible source is the very hot, optically thin plasma which forms in the cavity as a result of laser-plasma interaction. Its existence has already been inferred from the results of pinhole photography and also from time-resolved x-ray spectroscopy (see paper II). In addition, volume radia-

tion will be generated when the plasma ablated by the x rays at the wall reaches the center of the cavity. We have attempted to assess the relative importance of wall and volume radiation through dedicated experiments and through a detailed analysis of the measured spectra.

Figure 7(a) shows spectra obtained with a large cavity (1 mm diameter), irradiated with $\lambda = 1.3$-μm laser light. The cavity had two diagnostic holes and part of its wall cut away such that the line of sight from the TGS would end either on the wall or pass freely through the cavity

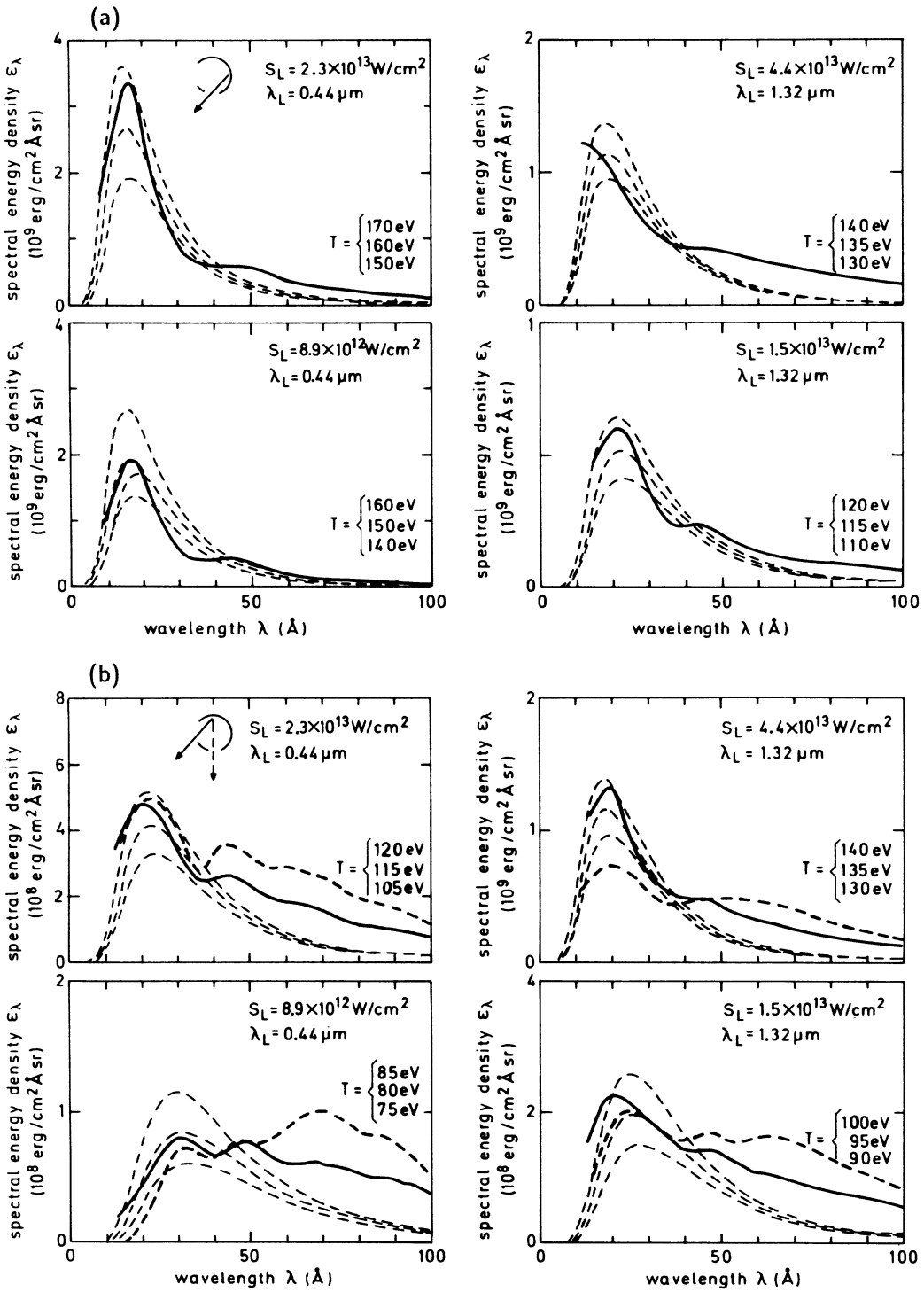

FIG. 6. Spectral energy density radiated by the cavity vs wavelength for 0.44- and 1.3-μm laser irradiation. S_L is the absorbed laser flux averaged over the inner surface of the cavity. Thin dashed lines are Planckian spectra calculated for a radiation time of 300 ps. (a) Radiation emitted from the back wall through the diagnostic hole. (b) Radiation emitted from the side wall through the laser hole (solid line) and through the diagnostic hole (dashed line).

[see inset of Fig. 7(a)]. It is seen that only a comparatively weak spectrum is observed if the wall is cut away. Thus the contribution from volume emission is small in such a large cavity. Also the spectrum peaks at long wavelengths ($\cong 80$ Å), suggesting that it is generated after laser irradiation when the temperature in the cavity has already decreased from its maximum value and the cavity fills with ablated plasma from the wall.

Smaller cavities have been investigated in the configuration of Fig. 1(b). As an example we present in Fig. 7(b) the spectra obtained along two different lines of sight. As shown in the inset of Fig. 7(b) these lines of sight (the corresponding spectral energy densities are called ϵ_2 and ϵ_4) are equivalent with respect to the symmetry of the cavity, except that one of them (ϵ_4) does not end on the cavity wall. The results shown in Fig. 7(b) were obtained with one of the smallest cavities (252 μm diameter) irradiated with $\lambda = 0.44$-μm laser light. It is seen that the relative contribution of the radiation registered along the line of sight passing freely through the cavity is more significant for such a small cavity. In the long-wavelength part (≥ 60 Å) the spectra obtained along the two lines of sight become nearly equally intense. This observation may indicate that the radiation emitted at long wavelengths comes to a large part from the plasma which fills the cavity during the cooling phase. The relative importance of this contribution should be larger in a small cavity because filling begins earlier at a higher temperature. In the wavelength range 20–60 Å both spectra are quite similar, although a slightly harder spectrum is observed along the line of sight passing freely through the cavity. For wavelengths < 20 Å this tendency becomes quite pronounced. Here we possibly see the signature of the hot laser-plasma interaction zone in the cavity which emits the x rays seen by the pinhole cameras through the wall of the cavity. In the intermediate range (20–60 Å) the similarity of the spectra could indicate that part of the radiation comes from hot material ablated by the radiation heat wave at the edges of the holes and at wall elements situated near the line of sight.

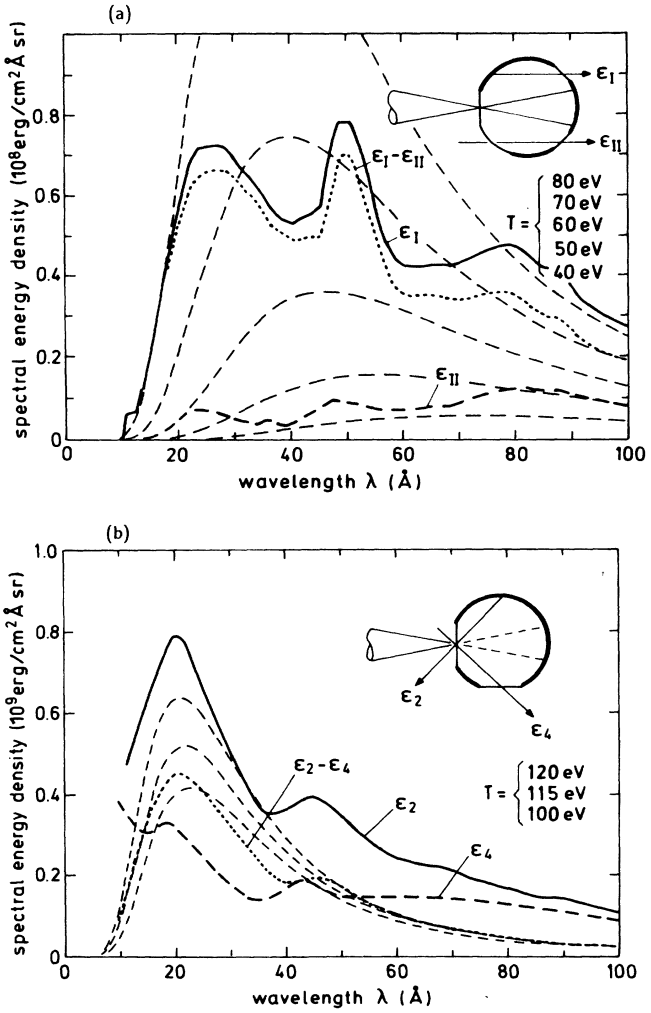

FIG. 7. (a) Spectra obtained simultaneously through two diagnostic holes (see inset) with either a radiating wall element present (ϵ_I) or absent (ϵ_{II}) along the line of sight (1-mm-diam cavity, 1.3-μm laser light, $S_L = 5\times10^{12}$ W cm^{-2}). (b) Spectra obtained through the laser hole (ϵ_2) or diagnostic hole (ϵ_4) with either (see inset) a radiating wall element present or absent (252-μm-diam cavity, 0.44-μm laser light, $S_L = 3\times10^{13}$ W cm^{-2}).

Another possibility to obtain information about the source of the x rays is to evaluate the profile of the energy density in the spectrum normal to the dispersion direction . Due to the spatial resolution provided by the pinhole TGS this profile contains information about the source. If the radiation comes from an optically thick layer on the wall which radiates according to Lambert's cosine law, the wall will appear equally bright for any observation direction, the observation hole will radiate uniformly and the transverse profile of the spectrum will be symmetric with respect to its center line. If the optical thickness of the radiating layer is not large or if the radiation comes from an optically thin volume radiator in the cavity, the observation hole will radiate nonuniformly in general because each line of sight has a different length in the radiating material. In this case one expects an asymmetry in the profile. We calculated profiles of the energy density in the spectrum for the cases of a thin radiating layer on the wall and for a homogeneous volume radiator filling out the cavity. Parameter of the calculations was the optical thickness τ of the radiating layer or of the volume radiator, respectively. Calculated profiles are given in the Appendix.

Figure 8 shows profiles of the energy density across the spectrum at fixed wavelengths in the interval 20–100 Å. The profiles were obtained by the three TGS in an experiment where a 551-μm-diam cavity was irradiated by laser light with a wavelength of $\lambda = 0.44$ μm. Because asymmetrical profiles might arise from irregularities of the grating, we plotted the two profiles obtained in positive and negative dispersion direction over each other. Each scan is normalized with respect to its peak energy density. Because for a perfect grating both scans should coincide, the deviations between the two scans allow a judgement of the accuracy of the measurements. As can be seen, the agreement is reasonably good but not perfect,

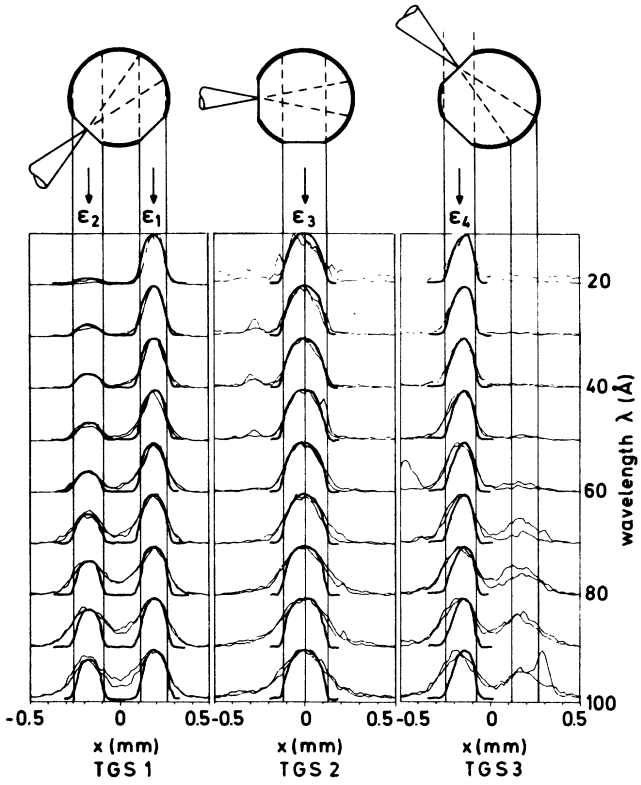

FIG. 8. Profiles of the energy density in the spectra normal to the dispersion direction at discrete wavelengths in the range 20–100 Å (551-μm-diam cavity, 0.44-μm laser light, $S_L = 6 \times 10^{12}$ W cm^{-2}). For the calculation of the profiles (thick solid lines) an optically thick wall radiator was assumed for ϵ_1, ϵ_2, and ϵ_3, and a uniform volume radiator with an optical thickness of 0.1 for ϵ_4.

and quality differences of the individual gratings may be recognized (film noise is usually not a limiting factor as may be judged from the noise observed on both sides outside the actual spectrum). The experimental scans are shown together with profiles which were calculated under the assumptions discussed below.

The side wall of the cavity is observed by TGS1 through the laser hole and by TGS2 through the diagnostic hole. The corresponding experimental profiles are shown together with profiles calculated for a wall radiator of infinite optical thickness. The comparison shows that the experimental and calculated profiles are in reasonable agreement for $\lambda < 50$ Å the experimental profiles become wider than the calculated ones. Previous investigations[6,10] have shown that this effect is pronounced for small, thin-walled (2 μm) cavities, but weak for large, thick-walled (40 μm) cavities. It is again attributed to the emission of radiation in the cooling phase of the cavity. For small, thin-walled cavities the diameter of the cavity and of the holes increases during the cooling phase as a result of outward acceleration of the cavity wall by x-ray ablation; in addition radiation leaks through the wall after a few nanoseconds.[10] Large, thick-walled cavities move comparatively slowly, no radiation can penetrate through the wall, and the diagnostic hole radiates with its original diameter during the cooling phase.

The calculations described in the Appendix suggest that the experimental profiles obtained by TGS1 in observation of the side wall should show an observable asymmetry if the optical thickness of the radiating wall layer is less than $\tau \leq 1-2$. From the absence of such an asymmetry for $\lambda < 50$ Å one is lead to the conclusion that the optical thickness is at least that large, unless the asymmetry would be compensated by an opposite asymmetry (see Appendix) due to a volume radiator in the cavity.

The laser-irradiated back wall of the cavity is observed by TGS1 through the diagnostic hole. The corresponding experimental profiles (ϵ_1) are again shown together with profiles calculated for a wall radiator of infinite optical thickness. For $\lambda < 50$ Å the experimental profiles correspond also approximately to the calculated ones although deviations due to nonuniformities of laser light irradiation of the observed wall element would not be surprising. For $\lambda > 50$ Å a widening of the profile is again observed, which is, as before, attributed to emission during the cooling of the cavity. It may also be noted in this context that the strong difference in intensity between the emission of the side wall and the laser-irradiated back wall seen in the spectrum of TGS1 for short wavelengths disappears more or less for the long wavelengths. This observation suggests also that for the emission at long wavelengths the cooling phase of the cavity is important because in the cooling phase (i.e., after the end of the laser pulse) the back wall is no longer distinct from any other wall element.

For the detection of volume radiation TGS3 is most suitable because the lines of sight passing through the diagnostic hole pass also through the laser hole without being intercepted by the wall. In this case the calculated profiles are for a volume radiator with an optical thickness $\tau = 0.1$ (along a ray through the center of the cavity) and are correspondingly slightly asymmetric. A slight asymmetry is also seen in the experimental profiles; however, only for short-wavelength x rays in the range 20–30 Å. Possibly we see here another signature of the hot volume radiator in the cavity. At longer wavelengths the profiles become broader as in the other spectra and this type of asymmetry can no longer be distinguished.

In paper III, where we compare experiment and theory, we shall assume that the observed radiation is generated at the wall of the cavity. In order to eliminate the contribution of volume radiation we shall base the comparison on the measured radiation from the side wall as observed through the laser hole but subtract the radiation measured along the symmetric line of sight through the laser and diagnostic hole [i.e., we use in the terminology of Fig. 7(b) the difference $\epsilon_2 - \epsilon_4$]. This procedure may somewhat underestimate the radiation from the ablative heat wave in the wall, because at least some of the radiation registered along the line of sight through laser and diagnostic hole may be generated by the expanding material of the ablative heat wave itself.

4. *Primary x-ray conversion efficiency*

The absorption measurements, x-ray pinhole photography, and optical shadowgraphy suggest that in the case of 0.44-μm irradiation a large part of the laser energy is absorbed at the back wall of the cavity and partly transformed into x rays. We have attempted to measure the x-ray conversion efficiency at the back wall through the diagnostic hole by the TGS1.

For the determination of the x-ray energy generated at the back wall the size of the emission area must be known. As the diagnostic hole was too small to observe the whole laser-heated area, its size has been measured from the diameter of the soft-x-ray emitting area observed at the outer side of the back wall by the TGS3. Figure 9 shows the ratio of the diameter of the luminous area to the nominal diameter of the laser-irradiated area. It is seen that the relative diameter of the luminous area increases in small cavities where the laser intensity is larger. This way of measuring the diameter of the heated area is applicable only to the 0.44-μm irradiation experiments, because only in this case a localized heating of the back wall is observed.

Figure 10 shows the x-ray conversion efficiency versus the incident laser flux. A correction was made for the fact that the laser irradiated area also receives and partly reemits x-ray radiation from the other wall elements of the cavity; for the conditions of the present experiment with a relatively small laser irradiated area this correction is however small. Figure 10 shows that the measured conversion efficiency is in the range 15–35 %.

5. *Brightness temperature*

From the measurements of the spectral energy density a brightness temperature can be derived if an assumption about the duration of the radiation emission is made. Here where we deal with time-integrated measurements we assume a universal radiation time of 300 ps, i.e., equal to the laser-pulse duration. Time-resolved measurements reported in paper II show a slightly longer radiation time of typically 550 ps. Based on this value the brightness temperature would be lower by a factor $(300/500)^{1/4} = 0.86$ than given here.

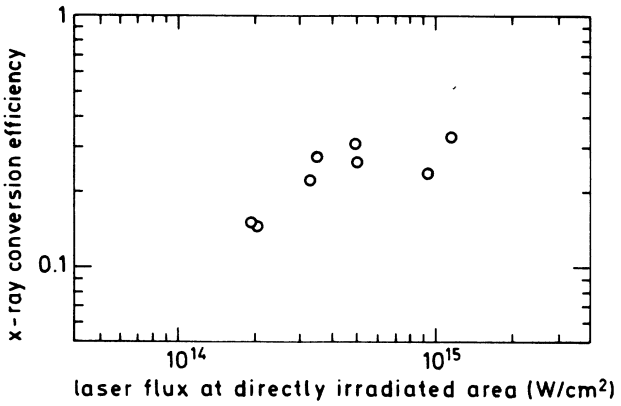

FIG. 10. Laser intensity dependence of the x-ray conversion efficiency at the back wall of the cavity (0.44-μm laser light).

The brightness temperature obtained in $\lambda = 0.44$-μm and $\lambda = 1.3$-μm irradiation experiments is shown in Fig. 11 versus the average absorbed laser flux. It is based on the quantity $\epsilon_2 - \epsilon_4$ [in terms of Fig. 7(b)], i.e., the contribution from the cavity volume is subtracted. It is seen that the brightness temperature depends only on the absorbed laser flux; no systematic dependence on the laser wavelength is observed. However, a rather large scatter occurs from shot to shot which remains unexplained at present. It may have to do with the subtraction of the zeroth order and the volume contribution (ϵ_4) which vary considerably from shot to shot. We note that in previous measurements[7] with photodiodes the scatter was much smaller. Another difference to our initial experiments is that a slightly higher temperature and a more reproducible behavior is found for the highest laser absorbed flux, i.e., the smallest cavities. The reason is that the small cavities in this initial series had been contaminated by residues of a cleaning agent (a Ce compound). The variable amount of impurities caused shot-to-shot fluctua-

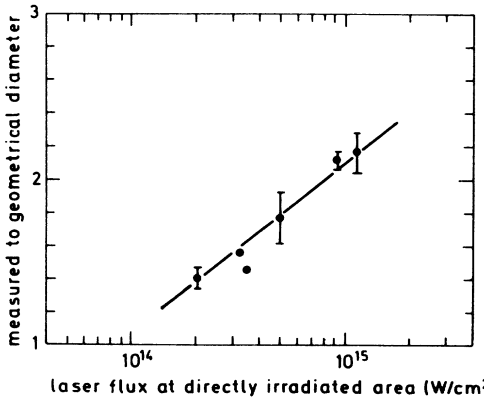

FIG. 9. Ratio of measured to geometrical diameter of the laser-irradiated area in the cavity (0.44-μm laser light).

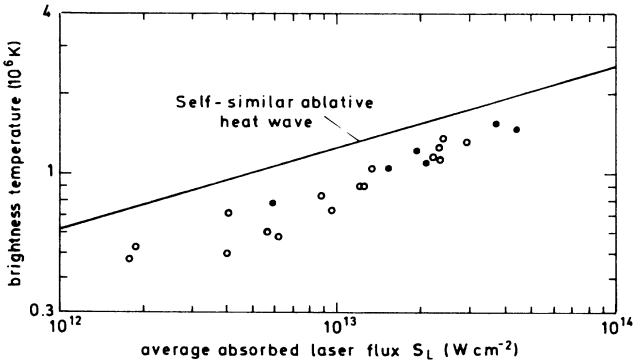

FIG. 11. Measured brightness temperature vs the average absorbed laser flux (○, 0.44-μm; ●, 1.3-μm laser light). The solid line represents the theoretical prediction on the basis of the self-similar ablative heat wave (see paper III or Ref. 7).

tions, modified (hardened) the spectrum and lowered the radiant energy flux in the cavity. Such impurities were carefully avoided in the present experiments.

According to our previous theoretical work[2,3] the temperature in the cavity is established in a balance between laser heating and radiative losses into the wall in the form of a self-similar heat wave.[43] We shall discuss the relation of theory and experiments in detail in paper III. However, for reasons of completeness and convenience, Fig. 11 shows also the theoretical prediction based on the self-similar ablative heat wave [from Eq. (1) in Ref. 7 or the identical Eq. (2a) in paper III]. As we shall see, the difference between experiment and theoretical prediction may be explained by the incomplete conversion efficiency in the cavity. Nevertheless, brightness temperatures up to about 1.5×10^6 K could be achieved in the cavities.

IV. SUMMARY

The simplest scenario of cavity heating in experiments with single-beam irradiation is the transformation of the laser light into x rays at the rear wall of the cavity. The x rays then heat the inner wall of the cavity. The experimental results suggest that this case is realized if the cavities are heated by short-wavelength $\lambda=0.44$-μm laser light. The existence of a well-defined laser-irradiated area is confirmed by x-ray pinhole photography, by optical shadowgraphy, and by direct spectral measurements through the diagnostic hole. The measurements suggest that about 15–35 % of the laser light is converted into x rays. The thermal radiation from the indirectly heated wall can be readily measured through the diagnostic hole without much contribution from the volume of the cavity, at least if the cavities are not too small. Excess radiation observed in the long-wavelength range $\lambda\geq40$ Å is attributed to the cooling phase of the cavity and is not unexpected. Brightness temperatures up to 1.5×10^6 K (corresponding to 130 eV) have been inferred for an input of absorbed laser light of $(2-3)\times10^{13}$ W cm^{-2}, averaged over the inner surface of the cavity.

With 1.3-μm irradiation of the cavities the situation is found to be much more complex. It appears that rapid plasma filling of the cavity strongly modifies the laser light path compared to an empty cavity. X-ray pinhole photography, optical shadowgraphy, and spectral measurements show consistently that the well-defined laser-irradiated area at the back wall does not exist in this case. The filling effect is so strong that 70% of the incident laser light is reflected by the smallest cavity. In addition the x-ray pinhole photographs show the emission of hard x rays from all over the cavity, most probably an indication for the generation of fast electrons during the nonlinear interaction of the infrared laser light with the plasma in the cavity. The observation shows many details of interest such as the formation of fine structures in the expanding material of the cavity wall or the formation of an x-ray emitting spot at the top of cavity. It seems plausible that these observations have to do with the generation of fast electrons. However, they need further investigation and interpretation.

As we have pointed out in the Introduction, a main purpose of this investigation was to identify the problems of cavity heating. It appears now that well-controlled cavity experiments require short-wavelength lasers; a fact already anticipated by the investigations reported in the literature with planar targets. It appears also (as we shall discuss in more detail in paper III of this investigation) that the level of thermal radiation generated in the cavity is at least in an approximate agreement with expectations, based on idealized models of cavity heating, although more accurate and detailed investigations of the steps leading to the thermalization of the laser light are clearly needed. Energetic short-wavelength laser pulses are likely to provide future progress in the cavity heating by laser.

ACKNOWLEDGMENTS

The authors would like to thank S. Witkowski for his continuous support and interest in this work and a critical reading of the manuscript and K. Eidmann for helpful discussions. The technical support by J. Bayerl, A. Böswald, H. Brändlein, W. Fölsner, and E. Wanka, and the operation of the Asterix Laser by H. Baumhacker, F. Denk, A. Herrle, and G. Keller are gratefully acknowledged. This work was supported in part by the Commission of the European Communities in the framework of the Association EURATOM–Max-Planck-Institut für Plasmaphysik.

APPENDIX: CALCULATION OF THE ENERGY DENSITY PROFILE IN THE SPECTRA

If the spectrum of the radiation emanating from the diagnostic hole of a cavity is registered on film with the help of a pinhole grating, the profile of the energy density in the spectrum at a given wavelength is determined by the geometrical configuration of the cavity with its diagnostic hole, the characteristics and distance of the pinhole grating, the distance to the film, and in addition by the properties of the source. Calculations of the energy-density profile for the case where the diagnostic hole is considered as blackbody radiator have been described earlier.[6] In the context of the present series of experiments we extended these calculations to include the effect of a finite optical thickness of the source.

Calculations were made for the two types of radiators in the cavity. One is a wall radiator with optical thickness τ. The other one is a uniform spherical volume radiator with an optical thickness τ along a diameter. For the two cases the spectral intensity is, respectively, given by

$$I_\lambda(\theta)=I_{\lambda P}(1-e^{-\tau/\cos\theta}) ,$$

$$I_\lambda(\theta)=I_{\lambda P}(1-e^{-\tau\cos\theta}) ,$$

where $I_{\lambda P}$ is the Planckian spectral intensity and θ is the angle between the normal of the observed wall element

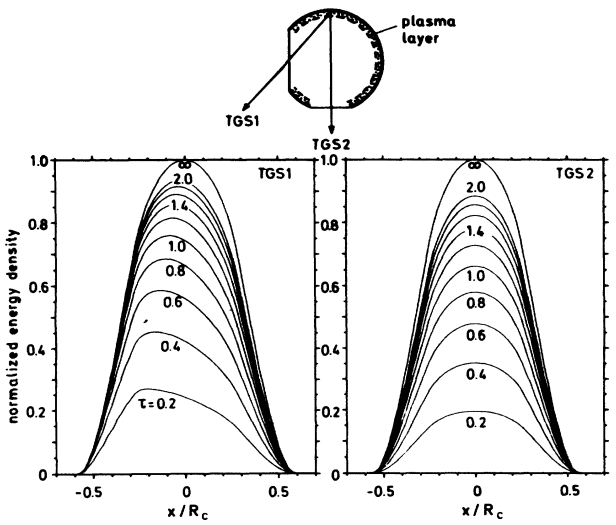

FIG. 12. Calculated profiles of the energy density in the spectrum normal to the dispersion direction. x/R_c is the transverse coordinate x divided by the cavity radius R_c. Parameter is the optical thickness τ of the radiator. The curves are normalized to the case $\tau=\infty$, i.e., to the profile expected for an optically thick blackbody radiator. The direction of observation corresponds to TGS1 (left) or TGS2 (right). The radiation comes from a thin plasma layer located on the inner wall of the cavity. The calculations were made for $R_L/R_c=0.6$, $R_D/R_c=0.4$, $R_p/R_c=0.083$, where R_L, R_D, and R_p are, respectively, the radii of the laser hole, diagnostic hole, and pinhole grating.

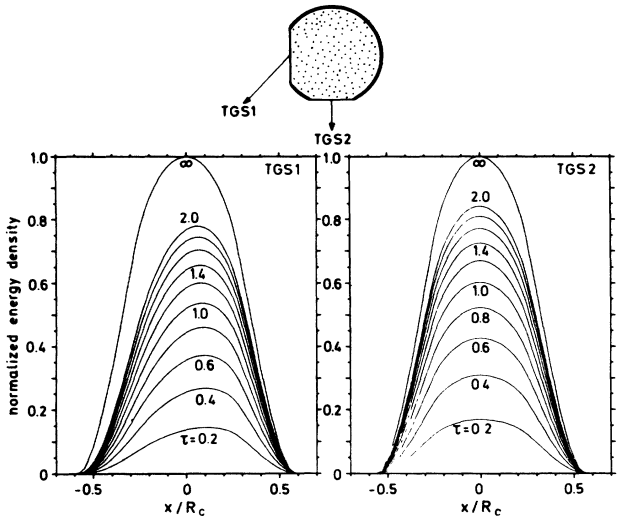

FIG. 13. Same as Fig. 12, however, for the case of a uniform volume radiator in the cavity.

and the direction of observation. The two types of radiators are shown together with the results in Figs. 12 and 13, respectively. As Figs. 12 and 13 show, the energy-density profile of a spectrum registered through the diagnostic hole by TGS2 is always symmetric in correspondence to the symmetry of the cavity configuration and observation direction. However, a spectrum registered through the laser hole by TGS1 will in general by asymmetric to an extent which depends on the optical thickness τ. It should be noted that the symmetries are opposite to each other for the two types of radiators and thus may cancel each other in the experiment. As τ is increased, the profiles converge towards the symmetric profile of a blackbody radiator.

*On leave from Institute of Laser Engineering, Osaka University, Suita Osaka, 565, Japan.
†On leave from Central Research Institute for Physics, H-1525 Budapest, Hungary.

[1]Ya. B. Zel'dovich and Yu. P. Raizer, *Physics of Shock Waves and High-Temperature Hydrodynamic Phenomena* (Academic, New York, 1966).
[2]R. Pakula and R. Sigel, Max-Planck-Institut für Quantenoptik Report No. MPQ 85, 1984 (unpublished).
[3]R. Pakula and R. Sigel, Z. Naturforsch. **41a**, 463 (1986).
[4]T. Mochizuki, S. Sakabe, K. Okada, H. Shiraga, T. Yabe, and C. Yamanaka, Jpn. J. Appl. Phys. **22**, L133 (1983).
[5]C. Yamanaka, H. Azechi, E. Fujiwara, S. Ido, Y. Izawa, T. Jitsuno, Y. Kato, Y. Kitagawa, N. Miyanaga, T. Mochizuki, S. Nakai, M. Nakatsuka, H. Niki, H. Nishimura, K. Nishihara, T. Norimatsu, T. Sasaki, S. Sakabe, T. Yabe, M. Yamanaka, T. Yamanaka, and K. Yoshida, in Proceedings of the Tenth International Conference on Plasma Physics and Controlled Nuclear Fusion Research held by the International Atomic Energy Agency, London, 1984 [Nucl. Fusion Suppl. **3**, 3 (1985)].
[6]R. Pakula, Max-Planck-Institut für Quantenoptik Report No. MPQ 95, 1985 (unpublished).
[7]P. Herrmann, R. Pakula, I. B. Földes, R. Sigel, G. D. Tsakiris, and S. Witkowski, Z. Naturforsch. **41a**, 767 (1986).
[8]G. D. Tsakiris, P. Herrmann, R. Pakula, R. Schmalz, R. Sigel, and S. Witkowski, Europhys. Lett. **2**, 213 (1986).
[9]I. B. Földes, K. Koyama, R. Sigel, G. D. Tsakiris, A. Böswald, Chen Shi-Sheng, A. G. M. Maaswinkel, R. F. Schmalz, and S. Witkowski, Europhys. Lett. **2**, 221 (1986).
[10]P. Herrmann, Max-Planck-Institut für Quantenoptik Report No. MPQ 118, 1986 (unpublished), in German.
[11]K. Okada, T. Mochizuki, N. Ikeda, M. Hamada, M. Mineo, R. Kodama, and C. Yamanaka, J. Appl. Phys. **59**, 2332 (1986).
[12]M. F. Rosen, D. W. Phillion, V. C. Rupert, V. C. Mead, W. L. Kruer, J. J. Thomson, H. N. Kornblum, V. W. Slivinsky, G. J. Caporaso, M. J. Boyle, and K. G. Tirsell, Phys. Fluids **22**, 2020 (1979).
[13]P. D. Rockett, W. Priedhorsky, and D. Giovanielli, Phys. Fluids **25**, 1286 (1982).
[14]W. C. Mead, E. M. Campbell, K. G. Estabrock, R. E. Turner, W. L. Kruer, P. H. Y. Lee, B. Prutt, V. C. Rupert, K. G. Tirsell, G. L. Stradling, F. Ze, C. E. Max, M. D. Rosen, and B. F. Lasinski, Phys. Fluids **26**, 2316 (1983).
[15]H. Nishimura, F. Matsuoka, M. Yagi, K. Yamada, S. Nakai, G. H. McCall, and C. Yamanaka, Phys. Fluids **26**, 1688 (1983).

[16]T. Mochizuki, T. Yabe, K. Okada, M. Hamada, N. Ikeda, S. Kiyokama, and C. Yamanaka, Phys. Rev. A **33**, 525 (1986).
[17]R. Kodama, K. Okada, N. Ikeda, M. Mineo, K. A. Tanaka, T. Mochizuki, and C. Yamanaka, J. Appl. Phys. **59**, 3050 (1986).
[18]S. R. Goldman and W. C. Mead, Nucl. Fusion **26**, 813 (1986).
[19]P. Alaterre, H. Pépin, R. Fabbro, and B. Faral, Phys. Rev. A **34**, 4184 (1986).
[20]K. Eidmann and T. Kishimoto, Appl. Phys. Lett. **49**, 377 (1986).
[21]H. N. Kornblum, R. L. Kauffman, and J. A. Smith, Rev. Sci. Instrum. **57**, 2179 (1986).
[22]P. D. Goldstone, S. R. Goldman, W. C. Mead, J. A. Cobble, G. Stradling, R. H. Day, A. Hauer, M. C. Richardson, R. S. Marjoribanks, P. A. Jaanimagi, R. L. Keck, F. J. Marshall, W. Seka, O. Barnouin, B. Yaakobi, and S. A. Letzring, Phys. Rev. Lett. **59**, 56 (1987).
[23]S. Sakabe, R. Sigel, G. D. Tsakiris, I. B. Földes, and P. Herrmann, Max-Planck-Institut für Quantenoptik Report No. MPQ 119, 1986 (unpublished).
[24]G. D. Tsakiris and R. Sigel, following paper, Phys. Rev. A **38**, 5769 (1988). Also, referred to in text as paper II.
[25]R. Sigel, R. Pakula, S. Sakabe, and G. D. Tsakiris, this issue, Phys. Rev. A **38**, 5779 (1988). Also, referred to in text as paper III.
[26]I. B. Földes, J. Bayerl, P. Sachsenmaier, and R. Sigel, Max-Planck-Institut für Quantenoptik Report No. MPQ 97, 1985 (unpublished).
[27]A. G. M. Maaswinkel, R. Sigel, H. Baumhacker, and G. Brederlow, Rev. Sci. Instrum. **55**, 48 (1984).
[28]K. Eidmann. T. Kishimoto, P. Herrmann, J. Mizui, R. Pakula, R. Sigel, and S. Witkowski, Laser Part. Beams **4**, 521 (1986).
[29]A. Bräuniger *et al.*, Appl. Opt. **18**, 368 (1979); **18**, 2906 (1979); **18**, 3502 (1979).
[30]T. Kishimoto, Max-Planck-Institut für Quantenoptik Report No. MPQ 108, 1985 (unpublished), in German.
[31]I. B. Földes, R. Pakula, S. Sakabe, and R. Sigel, Appl. Phys. B **43**, 117 (1987).
[32]A. Hasegawa, D. Daido, M. Fujita, K. Mima, M. Murakami, S. Nakai K. Nichihara, K. Terai, and C. Yamanaka, Phys. Rev. Lett. **56**, 139 (1986).
[33]H. Nishimura, H. Azechi, M. Nakai, S. Uchida, Y. Sakawa, T. Wada, H. Hasegawa, H. Sakurai, T. Yamanaka, and C. Yamanaka, Opt. Commun. **56**, 409 (1986).
[34]Y. Sakawa, K. A. Tanaka, H. Nishimura, M. Nakai, T. Yabe, H. Sakurai, Y. Izawa, Y. Kato, T. Mochizuki, M. Nakatsuka, and C. Yamanaka, Phys. Fluids **30**, 3276 (1987).
[35]I. B. Földes, R. Sigel, Chen Shi-sheng, K. Eidmann, R. F. Schmalz, G. D. Tsakiris, and S. Witkowski, Laser Part. Beams **6**, 123 (1988).
[36]O. Willi, P. R. Rumsby, C. Hooker, A. Raven, and Z. Q. Lin, Opt. Commun. **41**, 110 (1982).
[37]F. Amiranoff, K. Eidmann, R. Sigel, R. Fedosejevs, A. G. M. Maaswinkel, Yung-Lu Teng, J. D. Kilkenny, J. D. Hares, D. K. Bradley B. J. Macgowen, and T. J. Goldsack, J. Phys. D **15**, 2463 (1982).
[38]G. Thiell and B. Meyer, Laser Part. Beams **3**, 51 (1985).
[39]F. Schwirzke, J. Nucl. Mater. **128/129**, 609 (1984).
[40]F. Schwirzke, in *Laser Interaction and Related Plasma Phenomena,* edited by H. Hora and G. H. Miley (Plenum, New York, 1986), Vol. 7, p. 843.
[41]B. Grek, F. Martin, T. W. Johnston, H. Pépin, G. Mitchel, and F. Rheault, Phys. Rev. Lett. **41**, 1811 (1978).
[42]M. A. Yates, D. B. van Hulsteyn, H. Rutkowski, G. Kyrala, and J. U. Brackbill, Phys. Rev. Lett. **49**, 1702 (1982).
[43]R. Pakula and R. Sigel, Phys. Fluids **28**, 232 (1985); **29**, 1340(E) (1986).

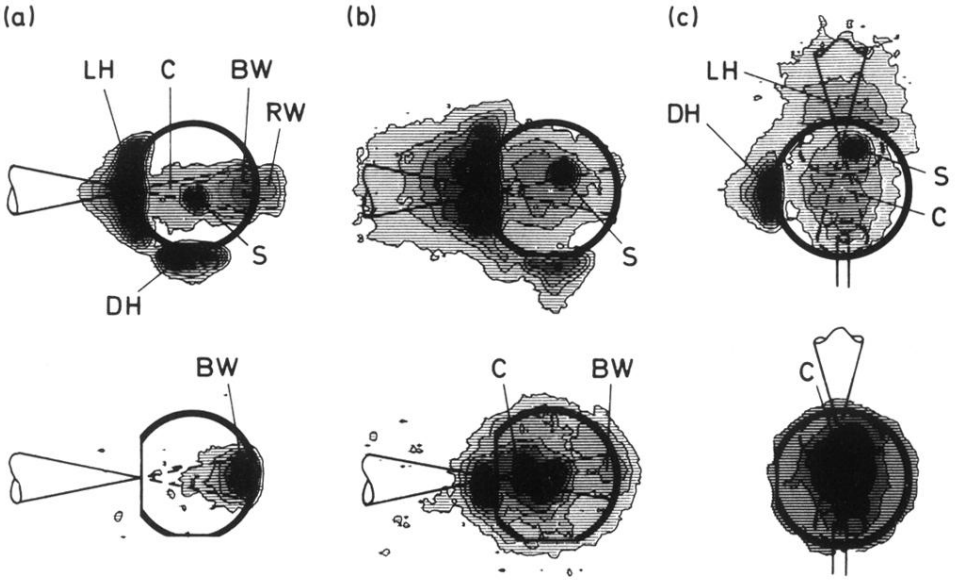

FIG. 3. X-ray pinhole photographs (isodensity contours) of laser-heated cavities. Upper row: Kodak 101-01 films exposed by relatively soft (0.7–3 keV) x rays. Lower row: SB2 films stacked behind the Kodak 101-01 film and exposed simultaneously by harder x rays (3–10 keV). For explanation of the symbols see text. (a) 297-μm-diam cavity heated by 0.44-μm laser light. Pinhole camera PHC1 (from top). Filter 1-μm-thick copper. Laser energy 24 J. (b) 328-μm-diam cavity heated by 1.3-μm laser light. Pinhole camera PHC1 (from top). Filter 1-μm-thick copper. Laser energy 63 J. (c) Same shot as (b); however, cavity observed by pinhole camera PHC2 (from rear side at 45° to the horizontal plane). Filter 1-μm-thick copper.

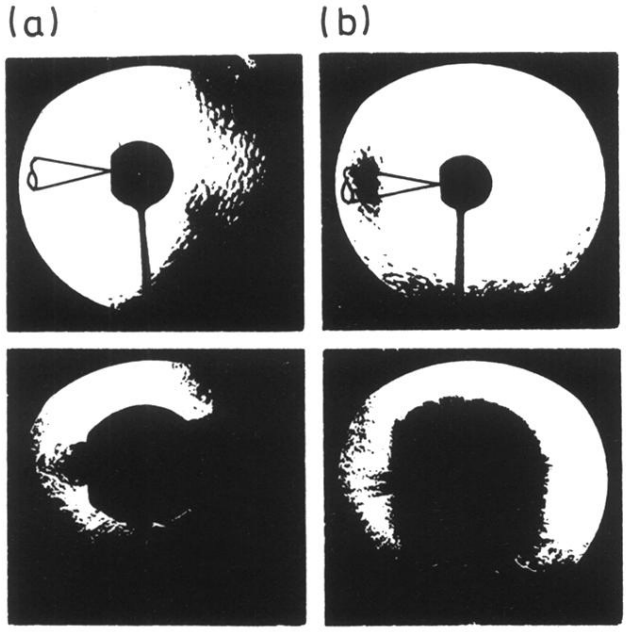

FIG. 4. Optical shadowgrams of two laser-heated cavities exposed by a dye-laser pulse ($\lambda = 0.58$ μm) of 3 ps duration. The cavities have a 2-μm-thick gold wall. Upper row: Cavity before irradiation. Lower row: Shadowgram of the expanding cavity 7 ns after the maximum of the heating laser pulse. (a) Cavity with 467 μm diameter heated by 0.44-μm laser light. (b) Cavity with 406 μm diameter heated by 1.3-μm laser light.

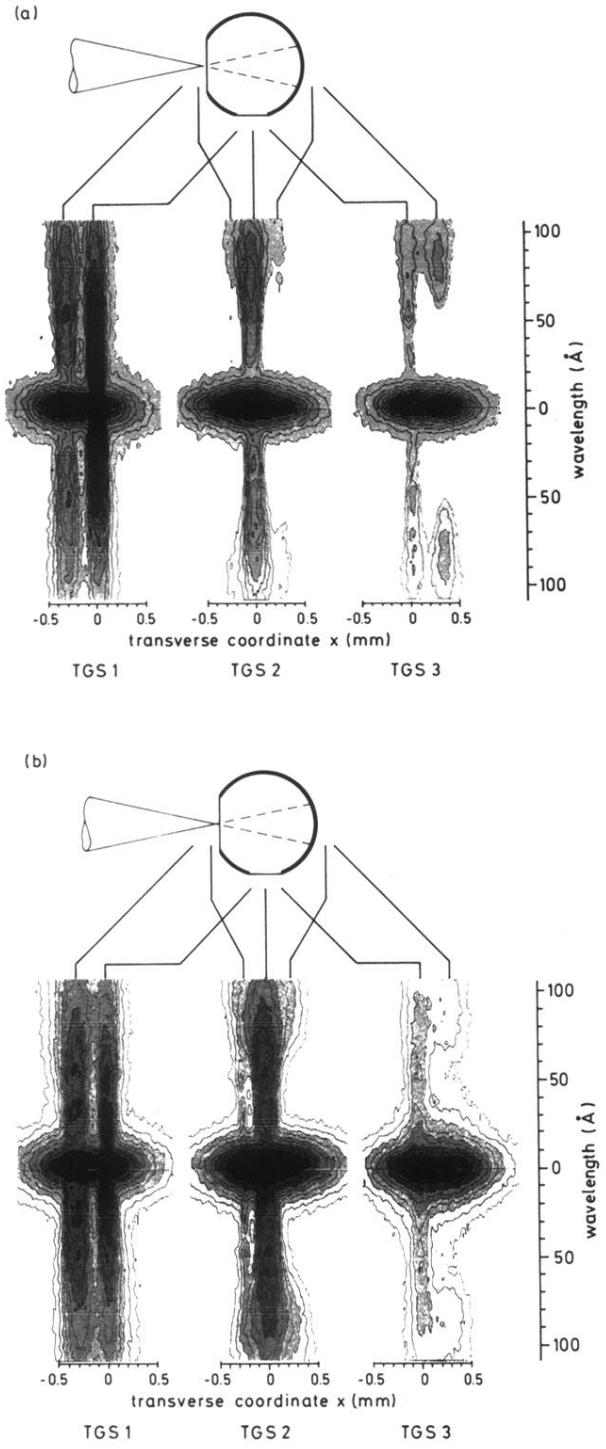

FIG. 5. Soft-x-ray spectra from laser-heated cavities registered by the three transmission grating spectrometers TGS 1–3 on Kodak 101-01 film. Shown are isodensity contours obtained by digitization and computer processing of the films. For clarity the spectra were stretched in the horizontal direction by a factor of 2. As a result the pinhole image of the diagnostic hole formed in zeroth order by the pinhole-grating combination appears elliptical rather than spherical. The transverse coordinate x gives distances in the plane of the cavity. (a) Cavity heated by 0.44-μm laser light (cavity diameter 467 μm, incident energy 22.9 J). (b) Cavity heated by 1.3-μm laser (cavity diameter 519 μm, incident energy 81.5 J).